Eur. Phys. J. Appl. Phys. (2013) 61: 10102
DOI: 10.1051/epjap/2012120318

THE EUROPEAN PHYSICAL JOURNAL APPLIED PHYSICS

Regular Article

Local current conduction due to edge dislocations in deformed GaN studied by scanning spreading resistance microscopy

Takashi Yokoyama[1], Yasushi Kamimura[1], Keiichi Edagawa[1,a], and Ichiro Yonenaga[2]

[1] Institute of Industrial Science, The University of Tokyo, Komaba, Meguro-ku, Tokyo 153-8505, Japan
[2] Institute for Materials Research, Tohoku University, Katahira, Sendai 980-8577, Japan

Received: 7 August 2012 / Received in final form: 12 November 2012 / Accepted: 23 November 2012
Published online: 14 January 2013 –

Abstract. Local electrical conductivities were measured for plastically deformed n-GaN single crystals by scanning spreading resistance microscopy (SSRM). In the SSRM images, many spots with high conductivity were observed, which can be attributed to introduced edge dislocations whose line direction is along [0 0 0 1] and Burgers vector is $\mathbf{b} = (a/3)[1\,\bar{2}\,1\,0]$. This result is in contrast to the previous studies which showed that grown-in edge dislocations of the same type in GaN films exhibit virtually no conduction. This suggests that the dislocation conduction depends sensitively on the dislocation core structure. Current-voltage spectra indicated a Frenkel-Poole mechanism for the conduction.

1 Introduction

Gallium nitride (GaN) and related nitride alloys have attracted tremendous attention in recent years as wide band gap semiconductors for applications in light-emitting diodes (LEDs) and laser diodes (LDs) in the blue and violet regions of the spectrum. In general, GaN thin films grown on foreign substrates contain a high density (10^7–10^9 cm^{-2}) of threading dislocations. In most cases, these threading dislocations are electrically active [1–12] and could degrade the device performance; they behave as nonradiative carrier-recombination sites, carrier scattering centers and leakage current paths. Dislocation charging in GaN has been studied by photoelectrochemical etching experiments [1], optical absorption experiments [2,3], scanning capacitance microscopy [4] and electron holography [5–7]. Several groups [8–12] have studied current leakage by dislocations in GaN films. These studies have shown that the threading dislocations of screw type are responsible for the current leakage [8–10], and that the conduction mechanism is of a Frenkel-Poole type [10–12]. Electronic-structure calculations by Northrup [13] have indicated that screw dislocations with the Burgers vector $\mathbf{b} = c[0\,0\,0\,1]$ in GaN can be highly conductive.

In the present study, we have investigated local current conduction due to dislocations in GaN by scanning spreading resistance microscopy (SSRM). To elucidate the intrinsic properties of dislocations, we introduced fresh dislocations by plastic deformation; grown-in dislocations are possibly decorated with native point defects or impurities during the growth process. We have found that edge dislocations introduced by deformation give high local conductivity, in contrast to the previous studies which showed that grown-in edge dislocations exhibit virtually no conduction. Local current-voltage (I-V) spectra have indicated a Frenkel-Poole mechanism for the conduction. Some of the preliminary results have already been reported elsewhere [14].

2 Experimental procedures

GaN single crystals with n-type carrier concentration of 5×10^{18} cm^{-3} doped with oxygen were grown by the hydride vapor phase epitaxy (HVPE) technique followed by the epitaxial lateral overgrowth (ELO) technique through SiO_2 masks on GaAs (1 1 1)A surfaces. Details of the growth technique and structural characterization of the crystals have been described elsewhere [15]. For compression tests, rectangular specimens with dimensions $1.0 \times 1.0 \times 3.6$ mm^3 were cut out from single crystals. The compression tests were conducted at 950 °C under a constant strain rate using an Instron-type machine. In Figure 1, the geometry of the crystal axes, the compression direction and the slip system are schematically shown together with the surface subjected to SSRM observations. Here, the primary slip system comprises the $(1\,0\,\bar{1}\,0)$ plane and the $[1\,\bar{2}\,1\,0]$ direction. The introduced shear strain was 5%. Detailed procedures of the deformation tests [16] and photoluminescence measurements [17,18] for the deformed samples have been reported elsewhere. After the deformation, some of the samples were sliced parallel to the glide plane followed by mechanical and ionic polishing, and observed by transmission electron microscopy (TEM)

[a] e-mail: edagawa@iis.u-tokyo.ac.jp

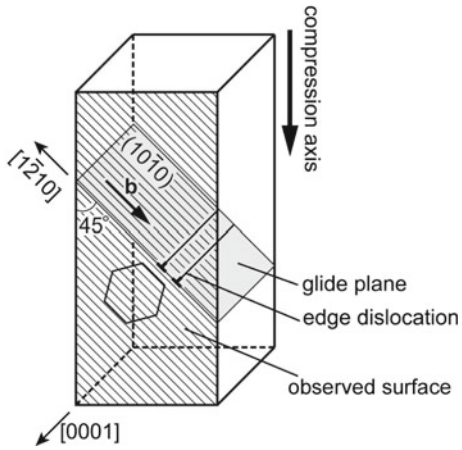

Fig. 1. The geometry of the crystal axes, the compression direction, the slip system and the surface subjected to SSRM observations.

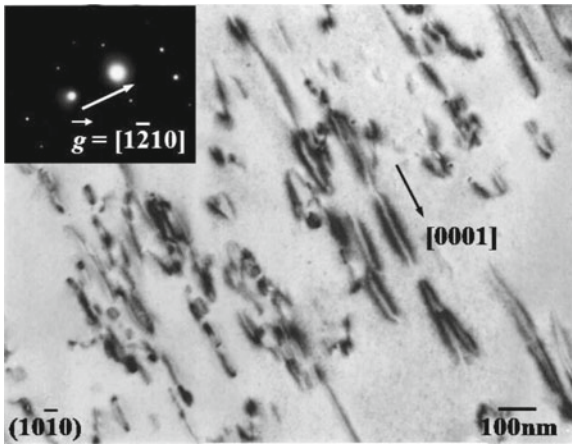

Fig. 2. A TEM bright-field image of a deformed sample.

to characterize the introduced dislocations. We also prepared an undeformed reference sample subjected to the same temperature history as that of the deformed samples. The (0 0 0 1) surfaces of both the deformed and the undeformed samples were first subjected to conventional mechanical polishing and subsequently to photoelectrochemical etching [19]. Local conductivities were measured on the (0 0 0 1) surfaces (see Fig. 1) by SSRM using a JEOL JSPM4200 microscope at room temperature according to the procedure described in our previous paper [20]. Here, a conductive diamond-coated Si cantilever or a Ti-Pt-coated Si cantilever was used, where the applied force was 1–5 μN. Ohmic contacts were formed on the back-side surfaces by depositing Ti/Al. Local current-voltage (I-V) spectra were also measured.

3 Results and discussion

Figure 2 shows an example of TEM bright-field image of a deformed sample, where a lot of straight dislocations are observed to run along the [0 0 0 1] direction. The $g\cdot b$ analyses showed that the Burgers vector of the dislocations is $\mathbf{b} = (a/3)[1\,\bar{2}\,1\,0]$, and thus it is of the pure-edge type. The dislocation density was estimated to be 10^9–10^{10} cm^{-2}.

Figures 3a–3d show typical SSRM images of the (0 0 0 1) surface of (Fig. 3a) undeformed and (Figs. 3b–3d) deformed samples. Here, we used a conductive diamond tip with the tip bias of +9 V. The images of 3b and 3c are from different positions on the same sample, and a part of the image in 3c is enlarged and shown in 3d. In all the images, bright spots with high conductivity are observed but their density is much higher in the deformed sample than in the undeformed one. The slip direction is indicated by an arrow in the image of 3b and the spots are aligned along this direction to form chains. The density of the spots is 10^9–10^{10} cm^{-2}, which is comparable to the dislocation density estimated by TEM observations. We found no apparent correspondence between the current images and the AFM topographic images simultaneously taken, indicating that the conductive spots do not originate in the surface roughness. From these facts, we can conclude that the spots in Figures 3b–3d correspond to the dislocations introduced by deformation. In Figure 3d, the radii of the spots are 20–30 nm. We found that these are typical radii of the spots, when observed by a fresh tip. Here, the radius of the contact area of the tip with the sample surface in our SSRM observations was estimated to be 20 nm, which should correspond to the spatial resolution limit. The observed spot size is approximately the same as this resolution limit, indicating that the actual size of the high conductivity area should be confined in a small region around the dislocation core. As shown in Figure 2, $\mathbf{b} = (a/3)[1\,\bar{2}\,1\,0]$, edge dislocations running along the [0 0 0 1] direction are dominantly introduced by deformation. This type of dislocation should terminate at the observed (0 0 0 1) surface (see Fig. 1). Thus, the spots observed for the deformed samples can be attributed to these edge dislocations.

Some groups [8–10] have performed conductive AFM or SSRM measurements for GaN thin films. They have found that grown-in screw dislocations with $\mathbf{b} = c[0\,0\,0\,1]$ give conductive spots in both forward and reverse bias conditions and that grown-in edge dislocations with $\mathbf{b} = (a/3)[1\,\bar{2}\,1\,0]$ and the line direction along [0 0 0 1] do not. This fact appears to be inconsistent with our result. We speculate that this is due to the difference in the core structure between deformation-induced fresh dislocations and grown-in dislocations possibly decorated with native point defects or impurities. Such decorations may passivate the dangling bonds arranged along the dislocation. It has also been shown that the electronic states associated with the dislocation in GaN change sensitively with the dislocation core structure [13,21]. Hsu et al. [8] have reported that the conductive spot intensity of the screw dislocation in GaN is many orders of magnitude higher in the samples grown under Ga-rich conditions in comparison to N-rich conditions. According to the density-functional calculations by Northrup [13], such a difference can be interpreted as due to the conductivity difference depending on the dislocation core structure. Also in the case of edge dislocations, their electronic structures have been

https://doi.org/10.1051/epjap/2012120318 Published online by Cambridge University Press

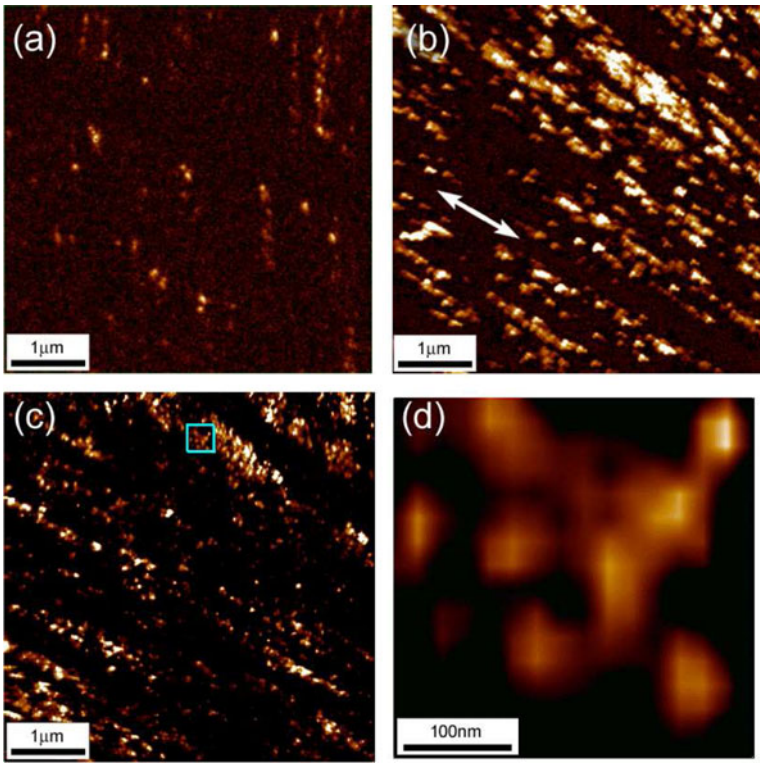

Fig. 3. (Color online) Typical SSRM images of the (0 0 0 1) surface of (a) undeformed and (b)–(d) deformed samples. Here, we used a conductive diamond tip with the tip bias of +9 V. The images of (b) and (c) are from different positions on the same sample, and an area indicated by a square in (c) is enlarged and shown in (d). The arrow in (b) indicates the slip direction.

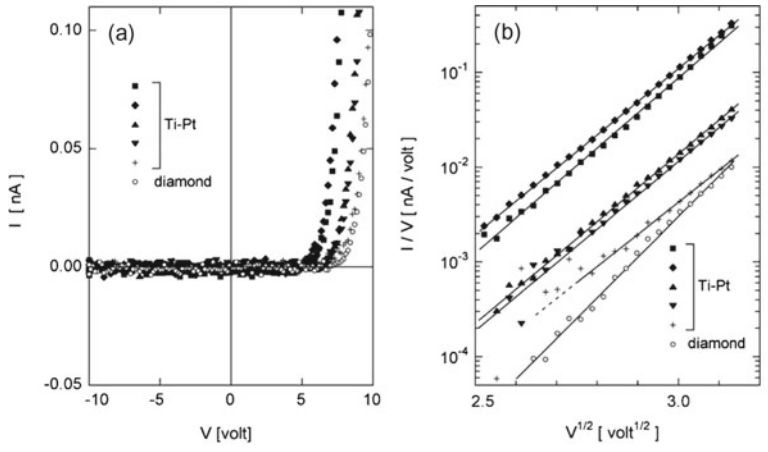

Fig. 4. (a) Local (I-V) spectra measured at the positions of conductive spots in SSRM images using a conductive diamond-coated tip and a Ti-Pt-coated tip, (b) the data in (a) are re-plotted as $\log(I/V) - V^{\frac{1}{2}}$.

theoretically shown to change sensitively with the core structure [21], which should result in a large difference in the conductivity.

Figure 4a shows local I-V spectra measured at the positions of conductive spots in SSRM images using a conductive diamond-coated tip and a Ti-Pt-coated tip. These spectra have been taken from different conductive spots. All the spectra show a clear rectifying behavior. We have analyzed the forward bias data in terms of various conduction mechanisms to find that the data can be fitted best to the Frenkel-Poole mechanism [22]. The Frenkel-Poole mechanism refers to a conduction mediated by carrier-trap states, which gives the I-V relation of the form [11,12]:

$$I = AV \exp\left[-\frac{q\left(\phi_t - B\sqrt{qV/\pi\varepsilon_0\varepsilon_s}\right)}{kT}\right]. \quad (1)$$

Here, q is the electron charge, ϕ_t is the barrier height for electron emission from the trapped state, ε_0 is the permittivity of free space, ε_s is the relative dielectric permittivity, kT has the usual meaning, and A and B are constants. Equation (1) predicts a linear $\ln(I/V) - \sqrt{V}$ relation, i.e.,

$$\ln(I/V) = \alpha + \beta\sqrt{V} \quad \text{with} \quad \alpha = \ln A - \frac{q\phi_t}{kT}$$
$$\text{and} \quad \beta = \frac{qB\sqrt{q/\pi\varepsilon_0\varepsilon_s}}{kT}. \quad (2)$$

In Figure 4b, the forward bias data are re-plotted as $\log(I/V) - \sqrt{V}$, where we indeed find the linear dependences. The re-plotted data show that α values in equation (2) differ largely depending on the selected conductive spots whereas the differences in β are small.

https://doi.org/10.1051/epjap/2012120318 Published online by Cambridge University Press

This indicates that the barrier heights ϕ_t for electron emission from the trapped state are different largely depending on the dislocation whereas the dielectric permittivities ε_s are effectively unchanged. There are various possibilities as to what kind of trap states are involved in the conduction. One is a trap state near the tip-sample interface; carriers that run along the dislocation come to the interface, get trapped by the states near the interface and then emitted to the tip. Another possibility is a trap state within the dislocation. For example, kinks in the dislocation may serve as carrier-trap sites. In fact, the dislocations introduced by deformation should have more kinks than those in the as-grown film.

Grown-in screw dislocations in GaN films have previously shown to exhibit a Frenkel-Poole conduction in forward bias [10] and in reverse bias [11,12]. Recently, Amma and his coworkers [23] have fabricated Al nanowires along threading dislocations of edge or mixed type in GaN films. They have shown that the conduction mechanism along these wires is also of a Frenkel-Poole type.

4 Conclusions

Local electrical conductivities were measured for plastically deformed n-GaN single crystals by scanning spreading resistance microscopy (SSRM). The dislocations introduced by deformation were of an edge type with $\mathbf{b} = (a/3)[1\,\bar{2}\,1\,0]$ and with the line direction along $[0\,0\,0\,1]$. In the SSRM images, many spots with high conductivity were observed. The spots are aligned along the slip direction to form chains. The density of the spots is comparable to the dislocation density estimated by TEM observations. From these facts, we can conclude that the spots are due to the edge dislocations introduced by deformation. This result is in contrast to the previous studies which showed that grown-in edge dislocations of the same type in GaN films exhibit virtually no conduction. This suggests that the dislocation conduction depends sensitively on the dislocation core structure. Current-voltage spectra indicated a Frenkel-Poole mechanism for the conduction, where the barrier heights for electron emission from the trapped state are different largely depending on the individual dislocation.

We thank Dr. K. Motoki of Sumitomo Electric Industries Ltd. for supplying the GaN bulk crystals. This work was financially supported by Grant-in-Aid for Scientific Research on Priority Areas "Nano Materials Science for Atomic Scale Modification 474" from Ministry of Education, Culture, Sports, Science and Technology (MEXT) of Japan.

References

1. C. Youtsey, L.T. Romano, I. Adesida, Appl. Phys. Lett. **73**, 797 (1998)
2. H. Hasegawa, Y. Kamimura, K. Edagawa, I. Yonenaga, J. Appl. Phys. **102**, 026103 (2007)
3. I. Yonenaga, Y. Ohno, T. Taishi, Y. Tokumoto, H. Makino, T. Yao, Y. Kamimura, K. Edagawa, J. Cryst. Growth **318**, 415 (2011)
4. P.J. Hansen, Y.E. Strausser, A.N. Erickson, E.J. Tarsa, P. Kozodoy, E.G. Brazel, J.P. Ibbetson, U. Mishra, V. Narayanamurti, S.P. DenBaars, J.S. Speck, Appl. Phys. Lett. **72**, 2247 (1998)
5. D. Cherns, C.G. Jiao, Phys. Rev. Lett. **87**, 205504 (2001)
6. J. Cai, F.A. Ponce, Phys. Stat. Sol. A **192**, 407 (2002)
7. E. Müller, D. Gerthsen, P. Brückner, F. Scholz, Th. Gruber, A. Waag, Phys. Rev. **B73**, 245316 (2006)
8. J.W.P. Hsu, M.J. Manfra, R.J. Molnar, B. Heying, J.S. Speck, Appl. Phys. Lett. **81**, 79 (2002)
9. B.S. Simpkins, E.T. Yu, P. Waltereit, J.S. Speck, J. Appl. Phys. **94**, 1448 (2003)
10. J. Spradlin, S. Dogan, J. Xie, R. Molnar, A.A. Baski, H. Morkoc, Appl. Phys. Lett. **84**, 4150 (2004)
11. H. Zhang, E.J. Miller, E.T. Yu, J. Appl. Phys. **99**, 023703 (2006)
12. P.K. Rao, B. Park, S.-T. Lee, Y.-K. Noh, M.-D. Kim, J.-E. Oh, J. Appl. Phys. **110**, 013716 (2011)
13. J.E. Northrup, Phys. Rev. B **66**, 045204 (2002)
14. Y. Kamimura, T. Yokoyama, H. Oiwa, K. Edagawa, I. Yonenaga, IOP Conf. Ser.: Mater. Sci. Eng. **3**, 012010 (2009)
15. K. Motoki, T. Okahisa, N. Matsumoto, M. Matsushima, H. Kimura, H. Kasai, K. Takemoto, K. Uematsu, T. Hirano, M. Nakayama, S. Nakahata, M. Ueno, D. Hara, Y. Kumagai, A. Koukitu, H. Seki, Jpn J. Appl. Phys. Part 2 **40**, L140 (2001)
16. I. Yonenaga, K. Motoki, J. Appl. Phys. **90**, 6539 (2001)
17. I. Yonenaga, S. Itoh, T. Goto, Physica B **340–342**, 484 (2003)
18. I. Yonenaga, H. Makino, S. Itoh, T. Goto, T. Yao, J. Electron. Mater. **35**, 717 (2006)
19. C. Youtsey, I. Adesida, L.T. Romano, G. Bulman, Appl. Phys. Lett. **72**, 560 (1998)
20. T. Yokoyama, R. Takenaka, Y. Kamimura, K. Edagawa, I. Yonenaga, Appl. Phys. Lett. **95**, 202108 (2009)
21. A.F. Wright, U. Grossner, Appl. Phys. Lett. **73**, 2751 (1998)
22. S.M. Sze, *Physics of Semiconductor Device*, 2nd edn. (Wiley, New York, 1981)
23. S. Amma, Y. Tokumoto, K. Edagawa, N. Shibata, T. Mizoguchi, T. Yamamoto, Y. Ikuhara, Appl. Phys. Lett. **96**, 193109 (2010)

https://doi.org/10.1051/epjap/2012120318 Published online by Cambridge University Press